Research Article

Bai-Yun Zhao#, Jiao-Jiao He#, and Li Wang*

Adsorption/desorption performance of cellulose membrane for Pb(II)

https://doi.org/10.1515/gps-2023-0014
received January 27, 2023; accepted May 31, 2023

Abstract: Cellulose membrane (CM) was successfully prepared by phase conversion (L–S). The adsorption performance of CM for Pb(II) under different adsorption conditions was investigated, and the adsorption isothermal models and kinetic models were established. Additionally, desorption performance of CM for Pb(II) under different conditions were also investigated. Scanning electron microscope (SEM), energy dispersion spectroscopy (EDS), and Fourier transform infrared (FT-IR) methods were used to evaluate changes in the microstructure, element content, and functional groups of CM. The maximum adsorption capacity (343 $mg \cdot g^{-1}$) of Pb(II) was achieved (initial concentration of Pb(II) solution was 1,200 $mg \cdot L^{-1}$, pH was 4.5, adsorption time was 120 min, adsorption temperature was 30°C). Meanwhile, the process conforms to multi-molecular layer chemical adsorption. The desorption results showed that the maximum desorption capacity was 90.00 $mg \cdot g^{-1}$ (HNO_3 concentration was 0.04 $mol \cdot L^{-1}$, desorption time was 120 min, desorption temperature was 60°C). SEM showed that the pores were saturated after adsorption of Pb(II). Mapping and EDS analysis revealed that CM contained 72.14% Pb(II) after adsorption. In the FT-IR curve, Pb(II) chelated the C═O group of the CM. This method showed great potential for adsorption of Pb(II) from aqueous solutions.

Keywords: adsorption, cellulose, desorption, membrane, Pb(II)

1 Introduction

Lead ion (Pb(II)) wastewater is a common environmental pollutant in industry and human activities, which poses a serious threat to human health and ecological system. The presence of Pb(II) in water is due to releases and discharges from processes such as industrial production, mining, waste disposal, and use of lead products. The toxic effects of lead (II) on human body and environment are long-term and potential. In order to reduce the impact of Pb(II) wastewater on the environment and human health, it is necessary to control the discharge and pollution of Pb(II). In addition, scientific research and technological innovation play an important role in the development of efficient wastewater treatment methods to reduce the discharge of Pb(II) wastewater and protect the safety of water resources [1].

At present, it has been found that the main methods for treating heavy metals in water are adsorption, chemical precipitation, ion exchange, membrane filtration, etc. [2–6]. Among them, adsorption technology is widely used for its good treatment effect and simple operation [7,8].

Cellulose, a widely distributed renewable natural polymer compound, has the advantages of being economical, environmentally protected, and resistant to biological degradation. In recent years, cellulose membranes (CMs) have been commonly used in packaging, filtration, separation, and other fields [9–11]. In addition, the CM is also an adsorbent that facilitates the separation of contaminants from wastewater [12,13].

There were a large number of hydrogen bonds in cellulose, so the choice of solvent was the key to the preparation of CM. Currently, there are many main solvents for the dissolution of cellulose, including ionic liquid, cuprammonia solution, paraformaldehyde/dimethyl sulfoxide systems, etc. [14]. However, most of these solvents have the

# These authors contributed equally to this work.

*** Corresponding author: Li Wang,** College of Material Science and Art Design, Inner Mongolia Agricultural University, Laboratory of Fibrosis and Energy Utilization of Shrubby Resources in Inner Mongolia Autonomous Region, National Forestry Grassland Engineering Technology Research Center for Efficient Development and Utilization of Sandy Shrubs, Hohhot 010018, China,
e-mail: wlndcl@126.com, wl2083663@126.com
Bai-Yun Zhao, Jiao-Jiao He: College of Material Science and Art Design, Inner Mongolia Agricultural University, Laboratory of Fibrosis and Energy Utilization of Shrubby Resources in Inner Mongolia Autonomous Region, National Forestry Grassland Engineering Technology Research Center for Efficient Development and Utilization of Sandy Shrubs, Hohhot 010018, China

disadvantage of being toxic, environmentally unfriendly, and expensive. At present, scientists have found that alkali mixed solution has the advantages of environmental protection, low cost, simple operation, etc. Chen et al. [15] successfully prepared magnetic cellulose-based nanocomposite beads by using sodium hydroxide/urea aqueous to dissolve cellulose, and the adsorption performance of Pb(II) was studied. Duan et al. [16] prepared the CM using pre-cooled lithium hydroxide/urea solution to dissolve cellulose, improving tensile and thermal stability. The solubilities of cellulose from different sources in sodium hydroxide/urea were studied [17]. So far, CM using sodium hydroxide/urea/thiourea solution and their adsorption of Pb (II) has rarely been reported.

Herein CM was prepared by phase inversion method (L–S) with sodium hydroxide/urea/thiourea as the solvent system, and sulfuric acid (H_2SO_4) as the coagulation bath. The adsorption condition (initial concentration of Pb(II) solution, pH of Pb(II) solution, adsorption time, and adsorption temperature), kinetic models, isothermal models, and desorption conditions (HNO_3 solution concentration, desorption time, and desorption temperature) were explored. Finally, scanning electron microscope (SEM), mapping and energy dispersion spectroscopy (EDS), and Fourier transform infrared (FT-IR) were used to characterize the structure of CM, and the mechanism of adsorption of Pb(II) by CM was discussed.

2 Materials and chemical methods

2.1 Materials and instruments

Deionized water was used to prepare solutions such as Pb (II), hydrochloric acid, etc. The experimental reagents are shown in Table A2 (in Appendix), and the experimental instruments are shown in Table A3.

2.2 Preparation of CM

First, the cellulose mixed solution was prepared by the following conditions: the mass ratio of sodium hydroxide, urea, and thiourea with 8:8:6.5, the solution was frozen at −10°C. Subsequently, 5 g of cellulose was added to the mixed solution in an ice-water bath and stirred for 1 h to dissolve the cellulose. Next the homogeneous and transparent mixed solution was added to the culture dish containing a 7% H_2SO_4 coagulation bath. Finally, the substance was cured at 40°C for 2 h, washed with deionized water, lyophilized, and bagged for use.

2.3 Adsorption experiment

First, 50 mL of Pb(II) solution was added to a stopper conical flask (100 mL). The pH was adjusted to a specific value with a buffered solution (HCl solution or NaOH solution). 0.1 g of CM was added to the above solution. Subsequently, the flask was placed in a temperature oscillator (150 rpm·min^{-1}) at a certain temperature (20°C, 30°C, 40°C, 50°C, and 60°C) for a certain time (15, 30, 60, 120, and 180 min). The mixed solution was centrifuged for 5 min in a centrifuge (6,000 rpm·min^{-1}) after the adsorption reaction reached equilibrium. 1 mL of the Pb(II) solution, 1 mL of xylenol orange, 1.5 mL of hexamethylenetetramine, and 4 mL of phenanthroline were added to a 100 mL volumetric flask, conditioned with deionized water, the supernatant was measured at a wavelength of 574 nm by a double-beam UV-Vis spectrophotometer (TU-1901, Beijing Puxi General Instrument Co., Ltd), and Q_e was calculated using Eq. 1 as follows:

$$Q_e = \frac{(C_0 - C_e) \times V_1}{m_1} \quad (1)$$

where Q_e (mg·g^{-1}) is the adsorption capacity; C_0 (mg·L^{-1}) and C_e (mg·L^{-1}) are the concentrations of the Pb(II) solution before and after adsorption, respectively; V_1 (L) is the volume of Pb(II) solution; and m_1 (g) is the dosage of the CM.

2.4 Desorption experiment

50 mL of HNO_3 solution was added to a 100 mL conical flask. The concentrations were 0.01, 0.02, 0.03, 0.04, and 0.05 mg·L^{-1}, respectively. The saturated CM adsorbed by Pb(II) was placed in a conical flask and placed in an oscillator set at a constant temperature (30°C, 40°C, 50°C, 60°C, and 70°C) for a certain time (30, 60, 90, 120, 150, and 180 min). The mixed solutions were centrifuged for 3 min in the centrifuge (6,000 rpm·min^{-1}) after the desorption reaction. The supernatant was measured, and Q_t was calculated using Eq. 2 as follows:

$$Q_t = \frac{C_t \times V_2}{m_2} \quad (2)$$

where the desorption capacity is given by Q_t (mg·g^{-1}), the concentration of the Pb (II) solution is given by C_t (mg·L^{-1}), the volume of HNO_3 solution is given by V_2 (L), and the dosage of the adsorbed saturated CM is given by m_2 (g).

2.5 Characterization of samples

CM before and after the adsorption of Pb(II) was characterized and analyzed by SEM (6701F, Japan JSM Tld), EDS (bruker2000, Germany), and FT-IR (Tensor27, Germany).

3 Results and discussion

3.1 Adsorption performance of CM for Pb(II)

3.1.1 Initial concentration

The adsorption capacity increased rapidly at first and then tended to be flat with the increase in the initial concentration of Pb(II) solution (Figure 1a). The maximum adsorption capacity (343 mg·g^{-1}) was reached when the initial concentration was 1,200 mg·L^{-1}. Subsequently, the adsorption capacity increased slowly. Due to the increase in the initial concentration, the CM gradually reached saturation. Then, the adsorption sites of the CM were gradually occupied with the further increase in the Pb(II) concentration, and the adsorption capacity remained stable.

3.1.2 pH of Pb(II) solution

Adsorption capacity increases rapidly initially, and then decreases with pH increases (Figure 1b). When the pH was 4.5, the maximum adsorption occurred. When the pH was lower, hydrogen ions inhibited the chelation of C═O and N–H groups of the CM with Pb(II) [18]. The concentration of hydrogen ions in the solution decreased, the chelation of Pb(II) and CM increased, and the adsorption capacity increased. Subsequently, the hydroxide ions in the solution increased with the continuous increase in the pH, and the lead hydroxide precipitate was formed, resulting in the decrease in adsorption capacity.

3.1.3 Adsorption time

The adsorption capacity increased first and then tended to equilibrium with the extension of adsorption time (Figure 1c).

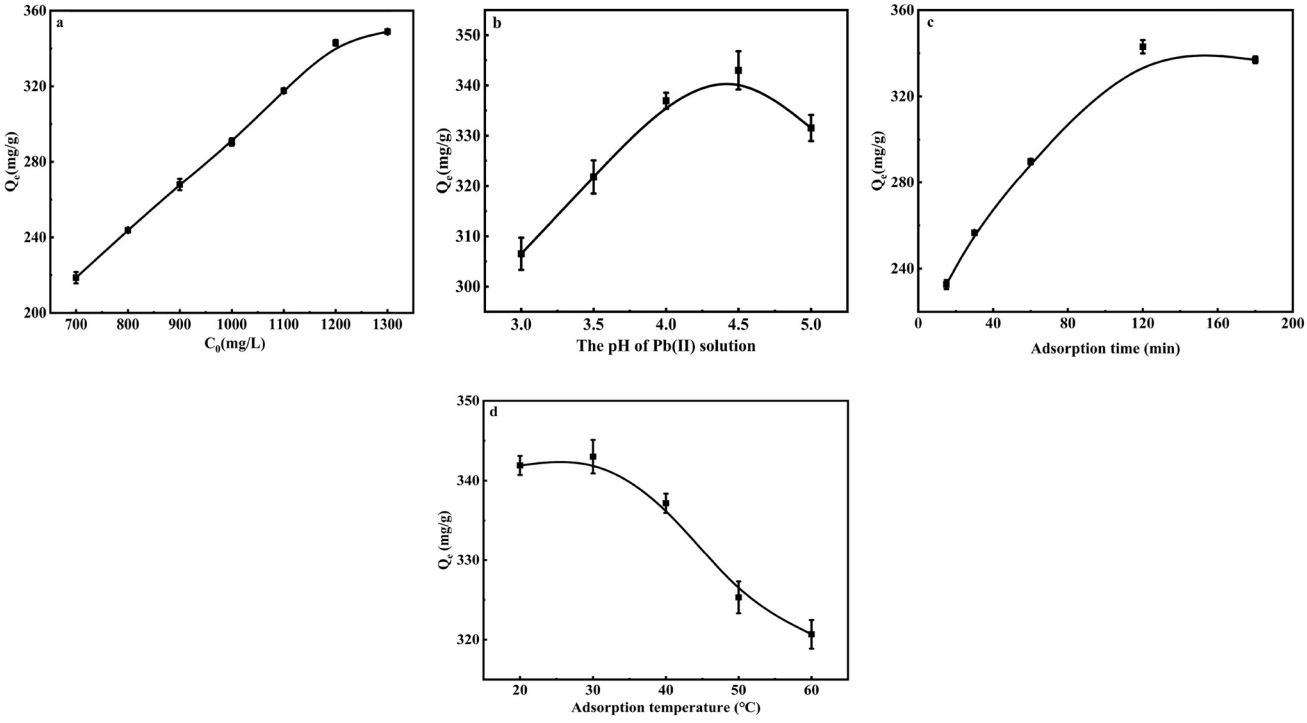

Figure 1: Adsorption capacity of CM for Pb(II) is affected by initial concentration of solution (a), pH (b), adsorption time (c), and temperature (d) of Pb(II) solution. (a) The pH of Pb (II) solution is 4.5, adsorption time is 120 min, and adsorption temperature is 30°C; (b) the initial concentration of Pb(II) solution is 1,200 mg·L^{-1}, adsorption time is 120 min, and adsorption temperature is 30°C; (c) the initial concentration of Pb (II) solution is 1,200 mg·L^{-1}, the pH of Pb(II) solution is 4.5, and adsorption temperature is 30°C; (d) the initial concentration of Pb(II) solution is 1,200 mg·L^{-1}, the pH of Pb(II) solution is 4.5, and adsorption time is 120 min.

The maximum adsorption capacity was reached when the adsorption time was 120 min. This was because the contact between the CM and Pb(II) was more adequate with the extension of adsorption time, resulting in the increase in adsorption capacity. However, the active site on CM tended to be saturated with the prolongation of adsorption time, and Pb(II) was no longer adsorbed. Finally, the adsorption capacity tended to be balanced.

3.1.4 Adsorption temperature

The adsorption capacity of Pb(II) by CM decreased with the increase in the adsorption temperature (Figure 1d). The maximum adsorption capacity was reached when the adsorption temperature was 30°C. This might be because the affinity of CM and Pb(II) decreased with the increase in the temperature, resulting in the decrease in adsorption capacity of CM for Pb(II) [19].

3.2 Adsorption isotherm models

Adsorption isotherms can well explain the relationship between Pb(II) and CM surface interaction. Adsorption data were analyzed by Langmuir [20] and Freundlich [21] isotherm models using Eqs. 3 and 4, respectively, as follows:

$$\frac{C_e}{q_e} = \frac{1}{(K_L \cdot q_{max})} + \frac{C_e}{q_{max}} \tag{3}$$

$$\ln q_e = \ln K_f + \frac{1}{n} \ln C_e \tag{4}$$

where the Pb(II) concentration in liquid phase equilibrium adsorption is given by C_e (mg·L^{-1}), the adsorption capacity in L–S equilibrium adsorption is given by q_e (mg·g^{-1}), the theoretical maximum adsorption capacity is given by q_{max} (mg·g^{-1}), the Langmuir and Freundlich constant are given by K_L (L·mg^{-1}) and K_f ((mg·g^{-1})·(L·mg^{-1})$^{1/n}$), respectively, and the adsorption strength is given by 1/n.

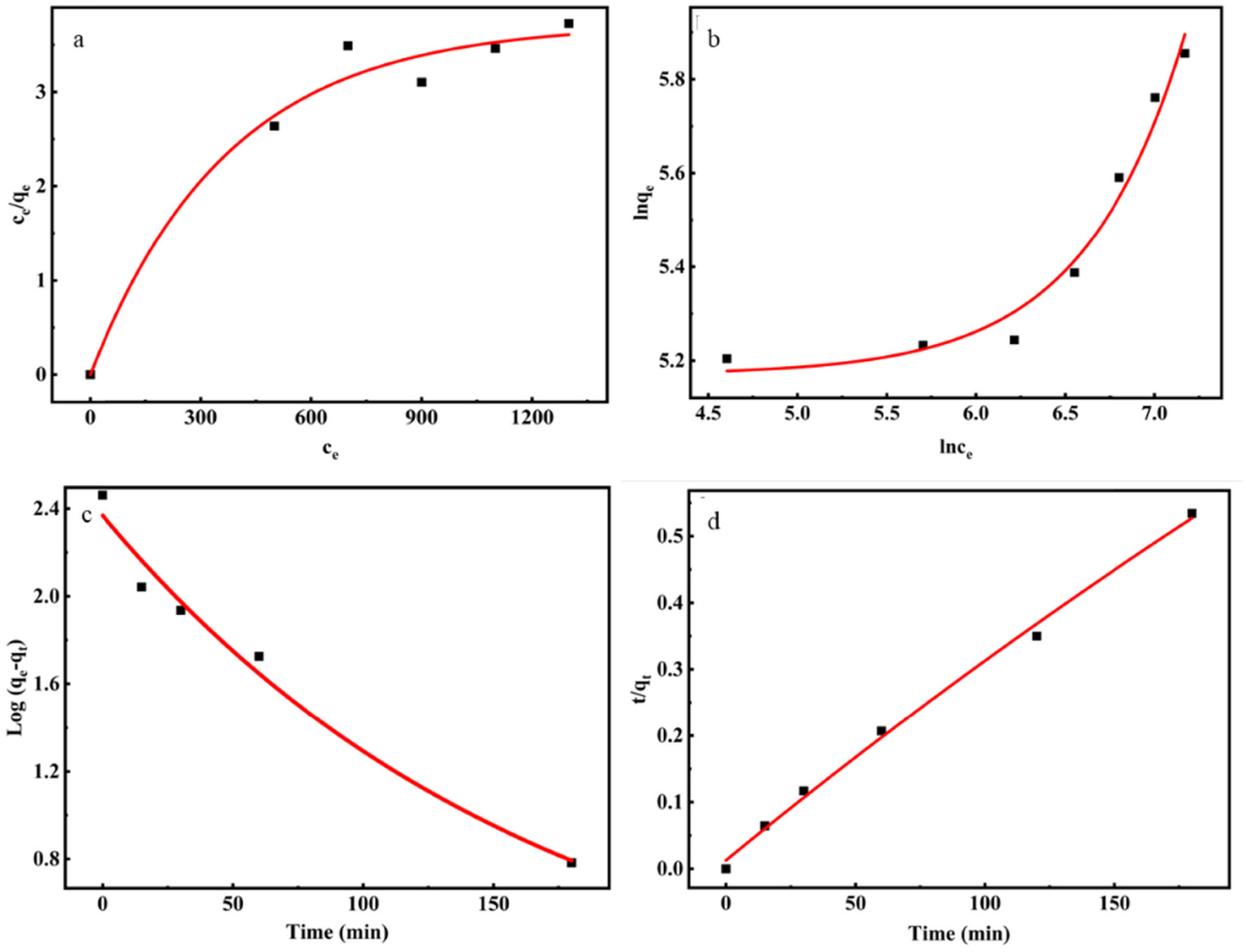

Figure 2: Langmuir (a) and Freundlich (b), pseudo-first-order (c), pseudo-second-order (d) models.

Table 1: Parameters of Langmuir and Freundlich isotherm models

Langmuir			Freundlich		
q_{max} (mg·g^{-1})	K_L (L·mg^{-1})	R^2	K_f ((mg·g^{-1}) (L·mg^{-1})$^{1/n}$)	1/n	R^2
372.7185	0.03414	0.9616	0.01168	0.5655	0.9618

The R^2 of the Langmuir and Freundlich isotherm models are 0.9616 and 0.9618, respectively (Figure 2a and b and Table 1). It could be seen that the adsorption of Pb(II) by CM coincided with the Langmuir and Freundlich isothermal adsorption models. Considering comprehensively, the adsorption process is multi-molecular layer adsorption. The n of Pb(II) adsorption by CM is 1.7638, since the value of n is greater than 1, it is indicated that the adsorption reaction is facilitated [21].

3.3 Adsorption kinetic models

The adsorption kinetic models reflect the adsorption rate of the CM and can better explain the adsorption mechanism of the CM in the Pb(II) solution. Two kinetic models are fitted to the data, pseudo-first-order [22] and pseudo-second-order [23] kinetic models, which are given by Eqs. 5 and 6, respectively, as follows:

$$\log (q_e - q_t) = \log q_e - \frac{k_1 t}{2.303} \quad (5)$$

$$\frac{t}{q_t} = \frac{1}{k_2 q_e^2} + \frac{t}{q_e} \quad (6)$$

where the adsorption capacity of the adsorption equilibrium and at time t are denoted by q_e (mg·g^{-1}) and q_t (mg·g^{-1}), respectively. The pseudo-first-order rate constant, pseudo-second-order rate constants are denoted by k_1 (min^{-1}) and k_2 (g·(mg·min)$^{-1}$), respectively.

The R^2 of the pseudo-first-order and pseudo-second-order kinetic models are 0.9601 and 0.9935, respectively (Figure 2c and d and Table 2). The R^2 is accords with the Pseudo-second-order kinetic model, and the progress is mainly chemisorption. It shows that this process is dominated by chemical adsorption, supplemented by physical adsorption.

3.4 Desorption performance of CM for Pb(II)

3.4.1 HNO_3 concentration

The desorption capacity of Pb(II) onto CM increased rapidly at first and then decreased with the increase in the HNO_3 concentration (Figure 3a). The maximum desorption capacity (90.00 mg·g^{-1}) was reached when the HNO_3 concentration was 0.04 mg·L^{-1}. At the same time, the desorption rate was lower (26.24%), indicating that the process of adsorption was mainly chemisorption (which was consistent with adsorption kinetics results). This was because the concentration of hydrogen ions increased with the concentration of HNO_3 increase, which competes with Pb(II) for adsorption sites, and the Pb(II) was desorbed from the CM [24]. The electrostatic repulsion between hydrogen ions and Pb(II) increases continuously with the increase in the concentration of HNO_3, resulting in the decrease in desorption capacity.

3.4.2 Desorption time

The desorption capacity of Pb(II) onto CM increased rapidly at first and then tended to equilibrium with the extension of desorption time (Figure 3b). The maximum desorption capacity was reached when the desorption time was 120 min. At the initial stage of desorption, there are more hydrogen ions in the solution, which compete with Pb(II) for adsorption and result in the Pb(II) falling off. Finally, the desorption progress reached a dynamic equilibrium with the prolongation of time, and the desorption capacity tended to balance.

3.4.3 Desorption temperature

The desorption capacity of Pb(II) onto CM increased rapidly at first and then tended to equilibrium with the rise of desorption temperature (Figure 3c). The maximum desorption capacity was reached when the desorption temperature was 60°C. The thermal motion of molecules accelerates with the rise in temperature, so that the adsorption saturated CM can obtain enough energy to desorb Pb(II), resulting in the increase in the desorption capacity [18]. However, the desorption

Table 2: Adsorption kinetic parameters of pseudo-first-order and pseudo-second-order models

Pseudo-first-order			Pseudo-second-order		
K_1 (min^{-1})	q_e (mg·g^{-1})	R^2	K (g·mg^{-1}·min^{-1})	q_e (mg·g^{-1})	R^2
0.0138	14.9555	0.9601	5.0649×10^{-5}	160.6836	0.9935

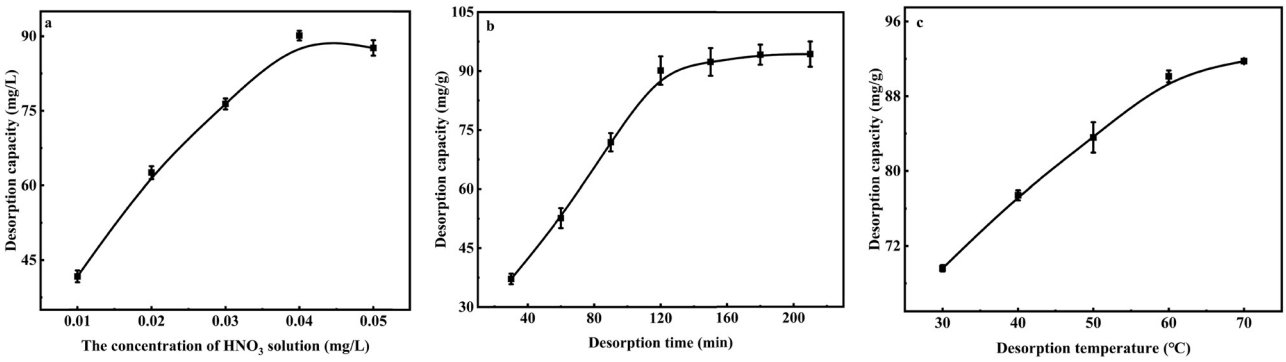

Figure 3: Desorption capacity of CM for Pb(II) is affected by HNO_3 concentration (a), desorption time (b), and desorption temperature (c). (a) The desorption time and desorption temperature are 120 min and 60°C, respectively; (b) the HNO_3 concentration is 0.03 mg·L^{-1}, the desorption temperature is 60°C; (c) the HNO_3 concentration is 0.03 mg·L^{-1}, the desorption time is 120 min.

reaction is difficult since the adsorption of Pb(II) by CM belongs to chemisorption (see Section 3.3).

3.5 Characteristics

3.5.1 SEM

The surface of the CM contains pores of different sizes (Figure 4a). The pores on the surface of the CM are filled with solid particles and become rough and dense after the adsorption of Pb(II) (Figure 4b). This indicated that Pb(II) have been successfully adsorbed to the CM surface (this result is consistent with that of EDS described in Section 3.5.2).

3.5.2 Mapping and EDS

The mapping images and EDS data of Pb(II) before (Figure 4c) and after (Figure 4d) adsorption of CM are shown in Figure 4 and Table 3. The CM did not contain Pb(II) before adsorption.

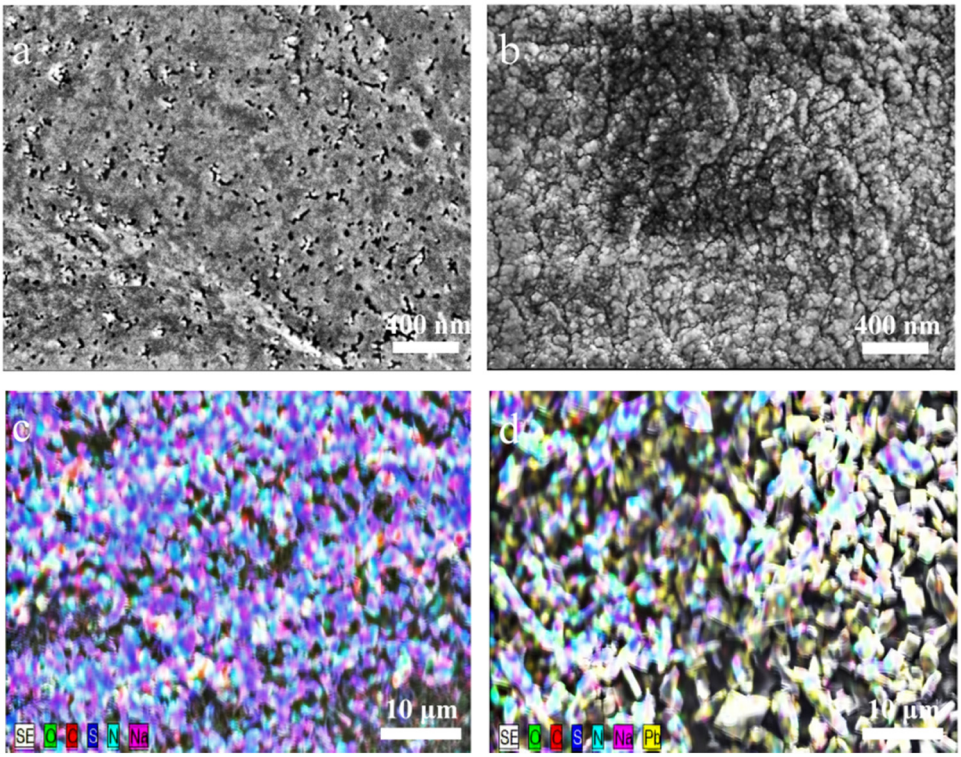

Figure 4: SEM images of CM before (a) and after (b) adsorption for Pb(II); mapping images of Pb(II) before (c) and after (d) adsorption.

Table 3: EDS data of Pb(II) before (a) and after (b) adsorption of CM

Element	a (wt%)	b (wt%)
C	13.43	3.84
O	50.58	13.27
N	4.95	0.74
S	17.15	9.52
Na	13.89	0.49
Pb	0	72.14

However, Pb(II) with higher content (72.14%) appeared on the CM after the adsorption reaction, demonstrating that Pb(II) was absorbed in the CM, and the CM had a strong adsorption capacity for Pb(II).

3.5.3 FT-IR

The characteristic absorption peak at 3,430 cm^{-1} was –OH peak [25] ("a" in Figure 5), and the intensity of the peak was weakened ("b" in Figure 5), which may be the reaction between –OH and Pb(II) [26]. The stretching vibration absorption peak of C═O in the carboxyl group and the N–H bending vibration absorption peak in the amino group were observed at 1,700 and 1,563 cm^{-1}, respectively. The two peaks disappeared indicating that the C═O group and the N–H group had a chelating effect on Pb(II). The bending vibration absorption peak of O–H in free water was observed at 1,635 cm^{-1} [27], and the peak moved to 1,633 cm^{-1}. The C–O and C–O–C stretching vibration absorption peaks were observed at 1,170 and 1,050 cm^{-1}, respectively [28,29]. The peaks of C–O and C–O–C were weakened, which may be due to the reaction between Pb(II) and cellulose, which reduced the ether bond in cellulose. The results show that the process of adsorption is mainly the formation of C═O and N–H groups and Pb(II). To sum up, the process of adsorption of Pb(II) onto CM is mainly due to the chelation between C═O, N–H groups, and Pb(II) [30]. It is proved that the adsorption belongs to chemical adsorption, which is consistent with the adsorption kinetics and desorption results (see Sections 3.3 and 3.4).

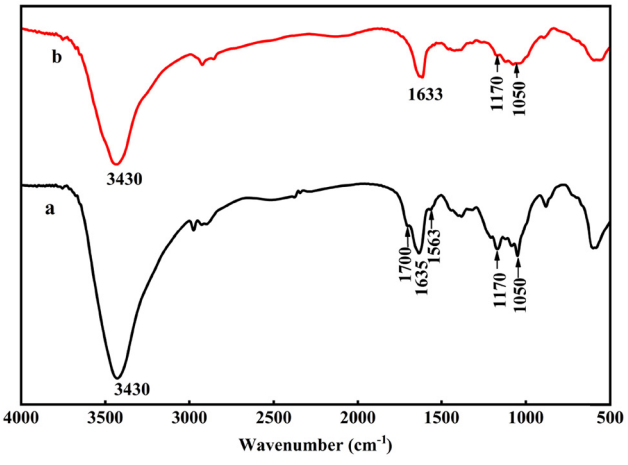

Figure 5: FT-IR spectra of CM for Pb(II) before (a) and after (b) adsorption.

3.6 Reaction mechanism

During the adsorption process, due to the existence of a large number of hydrogen bonds and carbonyl groups in CM, it might occur to adsorb Pb(II) in the solution (Eqs. 7 and 8).

$$2OH^{-}(CM) + Pb^{2+} \rightarrow Pb(OH)_2\downarrow \quad (7)$$

$$Pb^{2+} + 4C{=}O \rightarrow Pb(CO)_4 \quad (8)$$

4 Conclusion

CM was prepared by phase inversion method and applied to the adsorption of Pb(II) in wastewater. When the volume of Pb(II) solution was 50 mL, the dosage of CM was 0.1 g, the initial concentration of Pb(II) solution was 1,200 $mg{\cdot}L^{-1}$, the pH was 4.5, the adsorption time was 120 min, and adsorption temperature was 30°C, the adsorption capacity of the CM for Pb(II) could reach 343 $mg{\cdot}g^{-1}$. The fitting analysis of adsorption isotherm and adsorption kinetic model shows that the adsorption process of Pb(II) on CM belongs to multi-molecular layer chemical adsorption.

When the concentration of HNO_3 was 0.04 $mol{\cdot}L^{-1}$, desorption time and temperature were 120 min and 60°C, respectively. The desorption capacity of Pb(II) on CM could reach 90 $mg{\cdot}g^{-1}$. At the same time, it can be seen that the desorption rate is 26.24%, indicating that physical adsorption accounts for 26.24%.

The characterization results showed that the surface of CM contained many pores with different sizes, and the surface pores were filled during the adsorption process. C═O and N–H groups in CM chelate with Pb(II), which was beneficial to improving the adsorption capacity of CM for Pb(II). In addition, 72.14% Pb (II) appeared on the CM after adsorption. Therefore, the CM can not only improve the utilization rate of cellulose, but also has a

good adsorption performance for Pb(II), which provides a certain theoretical reference for the treatment of Pb(II)-containing wastewater.

Funding information: This work was financially supported by the Inner Mongolia Autonomous Region Natural Science Foundation Project (2016MS0210), the Inner Mongolia Autonomous Region Science and Technology Department Project (2019GG018), the Inner Mongolia Autonomous Region Natural Science Foundation Project (2021MS02024), and the Inner Mongolia Autonomous Region Science and Technology Department Project (2021GG0213).

Author contributions: Zhao Baiyun: writing – original draft, writing – review and editing, methodology, and formal analysis; He Jiaojiao: writing – original draft, formal analysis, visualization, and project administration; Wang Li: resources and funding acquisition.

Conflict of interest: The authors state no conflict of interest.

References

[1] Lin X, Shen T, Li M, Shaoyu J, Zhuang W, Li M, et al. Synthesis, characterization, and utilization of poly-amino acid-functionalized lignin for efficient and selective removal of lead ion from aqueous solution. J Clean Prod. 2022;347:131219. doi: 10.1016/J.JCLEPRO.2022.131219.

[2] Bin DOA, Saleh TA. Synthesis of polyamide grafted on biosupport as polymeric adsorbents for the removal of dye and metal ions. Biomass Convers. 2022:1–12. doi: 10.1007/S13399-022-02382-8.

[3] Saleh TA. Protocols for synthesis of nanomaterials, polymers, and green materials as adsorbents for water treatment technologies. Environ Technol Innov. 2021;24:101821. doi: 10.1016/J.ETI.2021.101821.

[4] Alkenani A, Saleh TA. Synthesis of amine-modified graphene integrated membrane as protocols for simultaneous rejection of hydrocarbons pollutants, metal ions, and salts from water. J Mol Liq. 2022;367(PB):120291. doi: 10.1016/J.MOLLIQ.2022.120291.

[5] Sani HA, Ahmad MB, Hussein MZ, Ibrahim NA, Musa A, Saleh TA. Nanocomposite of ZnO with montmorillonite for removal of lead and copper ions from aqueous solutions. Process Saf Environ Prot. 2017;109:97–105. doi: 10.1016/j.psep.2017.03.024.

[6] Abaszadeh M, Hosseinzadeh R, Tajbakhsh M, Ghasemi S. The synthesis of functionalized magnetic graphene oxide with 5-amino-1,10-phenanthroline and investigation of its dual application in C–N coupling reactions and adsorption of heavy metal ions. J Mol Struct. 2022;1261:132832. doi: 10.1016/J.MOLSTRUC.2022.132832.

[7] Hu Y, Gao H, Yang Q, Zhou W, Sun C. Adsorption of Pb^{2+} and Cd^{2+} on reduced graphene oxide hydrogel prepared from natural cryptocrystalline graphite. Colloids Surf. 2022;642:128630. doi: 10.1016/J.COLSURFA.2022.128630.

[8] Saleh TA. Global trends in technologies and nanomaterials for removal of sulfur organic compounds: Clean energy and green environment. J Mol Liq. 2022;359:119340. doi: 10.1016/J.MOLLIQ.2022.119340.

[9] He S, Fang H, Xu X. Filtering absorption and visual detection of methylene blue by nitrated cellulose acetate membrane. Korean J Chem Eng. 2016;33(4):1472–9. doi: 10.1007/s11814-015-0231-7.

[10] Cai Y, Chen D, Li N, Xu Q, Li H, He J, et al. Nanofibrous metal-organic framework composite membrane for selective efficient oil/water emulsion separation. J Membr Sci. 2017;543:10–7. doi: 10.1016/j.memsci.2017.08.047.

[11] Wang J, Zhao S, Dou P, Li X, Li D, He T. Sustainable fertilizer-drawn forward osmosis for the vegetable industry in reducing liquor from vegetable waste. Environ Technol. 2021;42(3):388–96. doi: 10.1080/09593330.2019.1629633.

[12] Zhang S, Chen H, Zhang S. Polyethylenimine grafted H_2O_2-oxidized cellulose membrane as a novel biosorbent for Cr(VI) adsorption and detoxification from aqueous solution. Cellulose. 2019;26(5):3437–53. doi: 10.1007/s10570-019-02325-z.

[13] Rafal S, Marcin M, Beata Z, Ewa T, Anna G. Graphene oxide/cellulose membranes in adsorption of divalent metal ions. RSC Adv. 2016;6(99):96595–605. doi: 10.1039/c6ra21432k.

[14] Anwar J, Niteen A, Dipak V. A critical review of manufacturing processes used in regenerated cellulosic fibres: viscose, cellulose acetate, cuprammonium, LiCl/DMAc, ionic liquids, and NMMO based lyocell. Cellulose. 2019;26(5):2913–40. doi: 10.1007/s10570-019-02318-y.

[15] Chen X, Chen J, You T, Wang K, Xu F. Effects of polymorphs on dissolution of cellulose in NaOH/urea aqueous solution. Carbohydr Polym. 2015;125:85–91. doi: 10.1016/j.carbpol.2015.02.054.

[16] Duan J, Obi Reddy K, Ashok B, Cai J, Zhang L, Varada R. Effects of spent tea leaf powder on the properties and functions of cellulose green composite films. J Environ Chem Eng. 2016;4(1):440–8. doi: 10.1016/j.jece.2015.11.029.

[17] Li R, Wang S, Lu A, Zhang L. Dissolution of cellulose from different sources in an NaOH/urea aqueous system at low temperature. Cellulose. 2015;22(1):339–49. doi: 10.1007/s10570-014-0542-6.

[18] Astrini N, Anah L, Haryadi HR. Adsorption of heavy metal ion from aqueous solution by using cellulose based hydrogel composite. Macromol Symp. 2015;353(1):191–7. doi: 10.1002/masy.201550326.

[19] Yan H, Rui W. Green recovery of lithium from water by a smart imprinted adsorbent with photo-controlled and selective properties. Chem Eng J. 2019;378:1–9. doi: 10.1016/j.cej.2019.122084.

[20] Zhao B, Yang X, Liu X, Shi Q, Liu Y, Wang L. Study on the cyclic adsorption performance of biomass composite membrane for Hg (II). Environ Technol. 2022. doi: 10.1080/09593330.2022.2071644.

[21] Wang D, Chen H, Zhang J, Li J. Easily synthesized mesoporous aluminum phosphate for the enhanced adsorption performance of U(VI) from aqueous solution. J Hazard Mater. 2022;432:128675. doi: 10.1016/J.JHAZMAT.2022.128675.

[22] Rind IK, Sarı A, Tuzen M, Lanjwani MF, Karaman I, Saleh TA. Influential antimony removal from aquatic solution using graphene nanoplatelet/*Staphylococcus aureus* as novel composite adsorbent. Surf Interfaces. 2023;38:102765.

[23] Wieszczycka K, Filipowiak K, Dudzinska P, Nowicki M, SiwińskaCiesielczyk K, Jesionowski T. Novel mesoporous organosilicas with task ionic liquids: Properties and high adsorption performance for Pb(II). Molecules. 2022;27(4):1405. doi: 10.3390/MOLECULES27041405.

[24] Zhou L, Zhou H, Hu Y, Yan S, Yang J. Adsorption removal of cationic dyes from aqueous solutions using ceramic adsorbents prepared from industrial waste coal gangue. J Environ Manage. 2019;234:245–52. doi: 10.1016/j.jenvman.2019.01.009.
[25] Saleh TA. Isotherm, kinetic, and thermodynamic studies on Hg(II) adsorption from aqueous solution by silica-multiwall carbon nanotubes. Environ Sci Pollut Res. 2015;22:16721–31. doi: 10.1007/s11356-015-4866-z.
[26] Saini S, Kumar R, Chawla J, Kaur I. Adsorption of bivalent lead ions from an aqueous phase system: Equilibrium, thermodynamic, kinetics, and optimization studies. Water Environ Res. 2019;91:1692–704. doi: 10.1002/wer.1180.
[27] Goh K, Ching Y, Chuah C. Individualization of microfibrillated celluloses from oil palm empty fruit bunch: comparative studies between acid hydrolysis and ammonium persulfate oxidation. Cellulose. 2016;23(1):379–90.
[28] Navid D, Kazem P, Vahabodin G, Ali S, Mohammad R. Systematically engineered electrospun conduit based on PGA/collagen/bioglass nanocomposites: The evaluation of morphological, mechanical, and bio-properties. Polym Adv Technol. 2019;30(9):2192–206. doi: 10.1002/pat.4648.
[29] Zhang H, Qian Y, Chen S, Zhao Y. Physicochemical characteristics and emulsification properties of cellulose nanocrystals stabilized O/W pickering emulsions with high -OSO_3- groups. Food Hydrocolloid. 2019;96:267–77. doi: 10.1016/j.foodhyd.2019.05.023.
[30] Anghel N, Marius N, Spiridon I. Heavy metal adsorption ability of a new composite material based on starch strengthened with chemically modified cellulose. Polym Adv Technol. 2019;30:1453–60. doi: 10.1002/pat.4577.
[31] Zhang N, Reguyal F, Praneeth S, Sarmah AK. A novel green synthesized magnetic biochar from white tea residue for the removal of Pb(II) and Cd(II) from aqueous solution: Regeneration and sorption mechanism. Environ Pollut. 2023;330:121806. doi: 10.1016/J.ENVPOL.2023.121806.
[32] Kim JG, Kim HB, Baek K. Novel electrochemical method to activate biochar derived from spent coffee grounds for enhanced adsorption of lead (Pb). Sci Total Environ. 2023;886:163891. doi: 10.1016/J.SCITOTENV.2023.163891.
[33] Danila V, Januševičius T. Adsorption of aqueous Pb(II) using non-devulcanized and devulcanized tyre rubber powder: A comparative study. Environ Sci Pollut Res. 2023. doi: 10.1007/S11356-023-27271-Z.
[34] Hao Z, Nie D, Zhang M, Wang W, Zou D, Nie G. Polymer-microsphere coated with MoS_2 nanoflowers for the removal of Pb(II) from water: Polydopamine-mediated MoS_2 assembly and efficient Pb(II) adsorption. Chem Eng J. 2023;465:142721. doi: 10.1016/J.CEJ.2023.142721.
[35] Wang Q, He D, Li C, Sun Z, Mu J. Honeycomb-like cork activated carbon modified with carbon dots for high-efficient adsorption of Pb(II) and rhodamine B. Ind Crop Prod. 2023;196:116485. doi: 10.1016/J.INDCROP.2023.116485.

Appendix

Table A1: Maximum adsorption capacity of Pb(II) onto different adsorbents

Adsorbents	Maximum adsorption capacity of Pb(II) ($mg \cdot g^{-1}$)	References
Biochar-based magnetic nanocomposite	81.6	[31]
Activate biochar	5.00	[32]
Non-devulcanized	75.1	[33]
Nanosized MoS_2-based adsorbents	371.7	[34]
Honeycomb-like cork activated carbon modified with carbon dots	231.48	[35]
CM	343	(In our study)

Table A2: Experiment chemical reagents

Chemical reagents	Chemical expression	Chemical reagents source
Cellulose	–	Hebei Bailingwei Superfine Materials Co., Ltd.
Sodium hydroxide	NaOH	Fu Chen (Tianjin) Chemical Reagent Co., Ltd.
O-Phenanthroline	$C_{12}H_8N_2$	Tianjin Fengchuan Chemical Reagent Technology Co., Ltd.
Hexamethylenetetramine	$C_6H_{12}N_4$	Tianjin Fengchuan Chemical Reagent Technology Co., Ltd.
Urea	CH_4N_2O	Tianjin Beilian Fine Chemicals Development Co., Ltd.
Methanol	CH_3OH	Tianjin Beilian Fine Chemicals Development Co., Ltd.
Ethanol	CH_3CH_2OH	Tianjin Beilian Fine Chemicals Development Co., Ltd.
Sodium sulfate	Na_2SO_4	Tianjin Beilian Fine Chemicals Development Co., Ltd.
Thiourea	CH_4N_2S	Tianjin Fu Chen Chemical Reagent Factory
Sulfuric acid	H_2SO_4	Tianjin Chemical Reagent No. 3 Factory
Nitric acid	HNO_3	Tianjin Chemical Reagent No. 3 Factory
Hydrochloric acid	HCl	Tianjin Chemical Reagent No. 3 Factory
Xylenol orange	$C_{31}H_{32}N_2O_{13}S$	Guoyao Group Chemical Reagent Co., Ltd.
Lead nitrate	$Pb(NO_3)_2$	Tianjin Shengao chemical reagent Co., Ltd.

Table A3: Instruments

Instruments	Model	Source
Dual-beam ultraviolet-visible spectrophotometer	TU-1901	Beijing Puxi General Instrument Co., Ltd, China
Centrifuge	H2050R	Changsha Xiangyi Centrifuge Instrument Co., Ltd, China
SEM	6701 F	Japan JSM company
FT-IR spectrometer	Tensor27	Bruker company of Germany